JACS
JOURNAL OF THE AMERICAN CHEMICAL SOCIETY
pubs.acs.org/JACS
Article

Interception of Transient Allyl Radicals with Low-Valent Allylpalladium Chemistry: Tandem Pd(0/II/I)−Pd(0/II/I/II) Cycles in Photoredox/Pd Dual-Catalytic Enantioselective C(sp^3)−C(sp^3) Homocoupling

Bo Li,[#] Hong-Hao Zhang,[#] Yongrui Luo, Shouyun Yu,* William A. Goddard III,* and Yanfeng Dang*

Cite This: *J. Am. Chem. Soc.* 2024, 146, 6377−6387
Read Online
ACCESS | Metrics & More | Article Recommendations | Supporting Information

ABSTRACT: We present comprehensive computational and experimental studies on the mechanism of an asymmetric photoredox/Pd dual-catalytic reductive C(sp^3)−C(sp^3) homocoupling of allylic electrophiles. In stark contrast to the canonical assumption that photoredox promotes bond formation via facile reductive elimination from high-valent metal−organic species, our computational analysis revealed an intriguing low-valent allylpalladium pathway that features tandem operation of Pd(0/II/I)−Pd(0/II/I/II) cycles. Specifically, we propose that (i) the photoredox/Pd system enables the in situ generation of allyl radicals from low-valent Pd(I)-allyl species, and (ii) effective interception of the fleeting allyl radical by the chiral Pd(I)-allyl species results in the formation of an enantioenriched product. Notably, the cooperation of the two pathways highlights the bifunctional role of Pd(I)-allyl species in the generation and interception of transient allyl radicals. Moreover, the mechanism implies divergent substrate-activation modes in this homocoupling reaction, suggesting a theoretical possibility for cross-coupling. Combined, the current study offers a novel mechanistic hypothesis for photoredox/Pd dual catalysis and highlights the use of low-valent allylpalladium as a means to efficiently intercept radicals for selective asymmetric bond constructions.

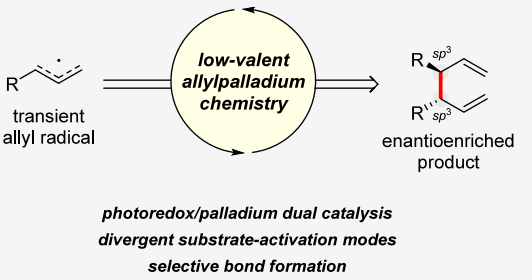

1. INTRODUCTION

Despite significant progress in the selective construction of carbon−carbon bonds, developing regio- and stereoselective catalytic methods for C(sp^3)−C(sp^3) coupling that generate vicinal stereocenters continues to be a major challenge in synthetic organic chemistry. Strategies such as transition-metal-catalyzed alkyl−alkyl cross-coupling between alkyl electrophiles and alkyl nucleophiles,[1−15] as well as reductive cross-electrophile coupling,[16−33] have evolved rapidly in recent decades. However, there is a need for advancing toward enantioconvergent and highly enantio- and diastereoselective processes that avoid stoichiometric alkyl metal/metalloid reagents or metal reductants. Additionally, although visible light photoredox chemistry has led to various powerful bond-formation protocols under mild and environmentally friendly conditions,[34−50] achieving effective enantioinduction in these reactions remains challenging. In this regard, we recently reported a photoredox/Pd dual-catalytic reductive homocoupling of allylic esters that provides a highly regio-, enantio-, and diastereoselective route to chiral C_2-symmetrical 1,5-diene scaffolds bearing vicinal stereogenic centers (Scheme 1A).[51] Although a series of experiments were designed and conducted to probe the reaction mechanism, the mode of catalysis and the origin of regio-/stereoselectivities remain largely unclear, which poses a significant barrier to subsequent reaction design efforts.

The initial working hypothesis of the photoredox/Pd dual catalysis involves the intermediacy of high-valent Pd(III) species to promote reductive elimination.[51,52] More specifically, it was proposed that interception of allyl radicals by Pd(II) species was responsible for the formation of Pd(III), which is in line with a plethora of studies on photoredox/transition-metal catalysis,[35−38,53−58] especially the prevailing postulate of reductive elimination from high-valent aryl-/acyl-/alkyl-Pd species at the Pd(III) or Pd(IV) states.[35,37,54−63] However, the high-valent mechanism cannot explain how the reaction avoids nonselective radical−radical coupling, which is a ubiquitous obstacle to regio-/stereocontrol in related nonreductive reactions.[59−64] This is in stark contrast to the remarkable regio- and stereoselectivites for the current reaction.[51,52] Moreover, a fundamental question remains regarding the possibility of cross-coupling under the reported

Received: January 21, 2024
Revised: February 10, 2024
Accepted: February 12, 2024
Published: February 22, 2024

Scheme 1. Photoredox/Pd Dual-Catalytic Homocoupling of Allylic Esters. (A) Reported reation.[51] (B) Current mechanistic study.

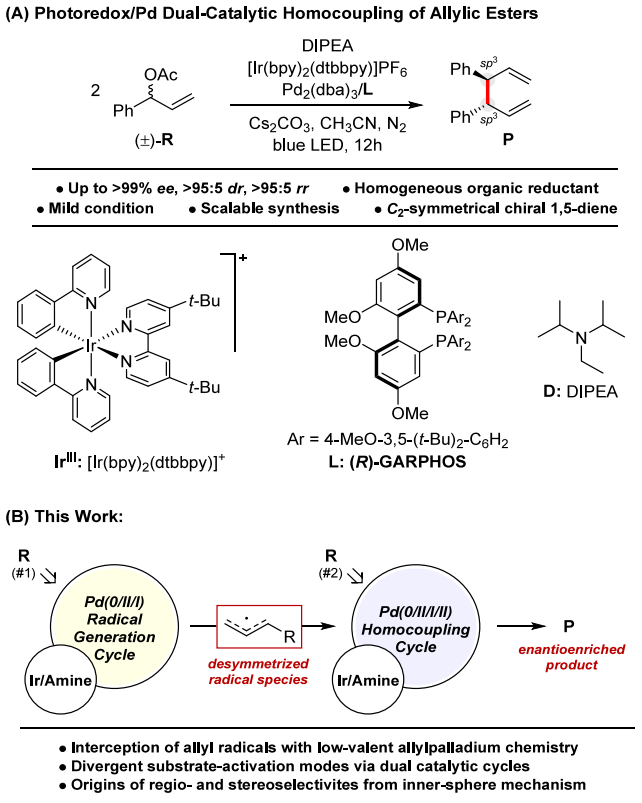

conditions. To this end, insights into the molecular nature of substrate activation and the resultant active species may help the differentiation of two substrates in one pot. To answer these questions, an in-depth theoretical survey into the intermediate (photo)redox events and the mechanism of catalysis is necessary.

We report herein quantum mechanics (QM) computations in tandem with experimental studies to establish the mechanism of photoredox/Pd dual catalysis (Scheme 1B). In contrast to the canonical high-valent regime, our computations reveal the operation of an underexplored low-valent allylpalladium chemistry, where a Pd(I) species (a) generates an allyl radical through a Pd(0/II/I) cycle and (b) efficiently intercepts the in situ-formed radical to enable the selective inner-sphere C(sp^3)−C(sp^3) bond construction in a separate Pd(0/II/I/II) cycle. We postulate that the enrichment of the chiral Pd(I) species by the reductive photoredox media is critical to the effective interception of the fleeting allyl radicals.[65] We also elucidate the transition-state origins of the unique reactivity and high selectivities. The study highlights the significant potential of low-valent allylpalladium chemistry as a new basis for the design of asymmetric photoredox/Pd dual catalysis.

2. COMPUTATIONAL METHODS

All quantum mechanical calculations were performed using the Gaussian 09 package.[66] For ground states and lowest triplet states, the M06-L functional was employed.[67,68] Geometries were optimized with a mixed SDD(Pd,Ir)-6-31G(d) basis set.[69,70] Optimized geometries were examined by vibrational frequency calculations to be either an energy minimum or a transition state (zero or one imaginary mode, respectively). Single-point energies were evaluated using the def2-TZVP basis set[71] and the SMD solvation model for CH_3CN.[72] Thermodynamic quantities (1 mol/L, 298.15 K) were calculated using the GoodVibes program[73] with the quasi-rigid rotor harmonic oscillator approximation.[74,75] Multiwfn[76] was employed for calculations of natural transition orbital (NTO),[77] Mayer bond order,[78] buried surface area,[79] steric contour,[80] and the independent gradient model.[81] Dispersion energies were estimated in the DFT-D3(BJ) scheme parametrized for the Hartree−Fock mean-field theory.[82] Visualizations were carried out in CYLview[83] and PyMOL.[84]

3. RESULTS AND DISCUSSION

The discussions are organized as follows. Section 3.1 describes the nature of the photoredox cycle. Section 3.2 presents a comprehensive computational analysis of the mechanism of catalysis for the photoredox/Pd dual catalysis, which highlights the pivotal role of low-valent allylpalladium in generating and intercepting allyl radicals for asymmetric homocoupling. Section 3.3 further establishes transition-state models that rationalize the selectivities and are then validated by experiments.

A standard reaction for the photoredox/Pd dual-catalytic reductive homocoupling is described in Scheme 1A.[51] Optimization of conditions identified [Ir(bpy)$_2$(dtbbpy)]PF$_6$ as an ideal photocatalyst, diisopropylethylamine (DIPEA or **D**) as a homogeneous organic reductant, Cs_2CO_3 as a necessary inorganic base, and (*R*)-GARPHOS (**L**) as a suitable ligand for enantioinduction. This highly reactive dual catalysis enables enantioconvergent consumption of racemic allylic esters. Up to >95:5 *rr*, >95:5 *dr* and 99% *ee* are observed for a variety of substrates, including the model substrate shown here, suggesting exceptional regio-, diastereo-, and enantiocontrol.

3.1. Photoredox Cycle. To establish the photochemical basis of the reaction, our studies commenced with an investigation into the initial fates of iridium photocatalyst $\mathbf{Ir^{III}}$ and organic reductant **D** (Figure 1A). The visible-light-induced reaction is triggered by photoexcitation of $\mathbf{Ir^{III}}$ toward $\mathbf{Ir^{III*}_{S1}}$, which displays characters of metal−ligand charge transfer (MLCT)/ligand π−π^* excitation (Figure S1). Vibrational relaxation of $\mathbf{Ir^{III*}_{S1}}$ and subsequent intersystem crossing (ISC) gives rise to the lowest triplet state $\mathbf{Ir^{III*}_{T1}}$, which shows an elevated thermodynamic potential (50.2 kcal/mol compared with the ground state $\mathbf{Ir^{III}}$), providing enhanced redox activities to engender the following reactions.

A previous analysis using a Stern−Volmer plot indicated that **D** ($E_{1/2}$ = +0.68 V vs SCE)[85−87] is responsible for quenching the photoexcited $\mathbf{Ir^{III}}$* species ($E_{1/2}$ = +0.66 V vs SCE).[88] In agreement with this observation, our calculations predict that the formation of $\mathbf{Ir^{III*}_{T1}}$ entails an exergonic reductive quenching by **D**, which involves a single-electron transfer (SET) from **D** to $\mathbf{Ir^{III*}_{T1}}$ to produce an $\mathbf{Ir^{II}}$ species and the $[\mathbf{D}]^{\bullet+}$ radical cation ($\Delta G_{SET}^{\ddagger}$ = 0.3 kcal/mol, ΔG_{SET} = −10.5 kcal/mol). $\mathbf{Ir^{II}}$ bears a radical anionic dtbbpy ligand (Figure 1B) and can act as a potent one-electron reductant. The formation of the radical cation $[\mathbf{D}]^{\bullet+}$ is followed by the deprotonation of $[\mathbf{D}]^{\bullet+}$ by Cs_2CO_3 (further exergonic by −23.7 kcal/mol). As also described in Figure 1B, the resultant radical **I**• is only one high-energy π^* electron away from a stable iminium cation, making it also a strong one-electron reductant. Additionally,

https://doi.org/10.1021/jacs.4c00676
J. Am. Chem. Soc. 2024, 146, 6377−6387

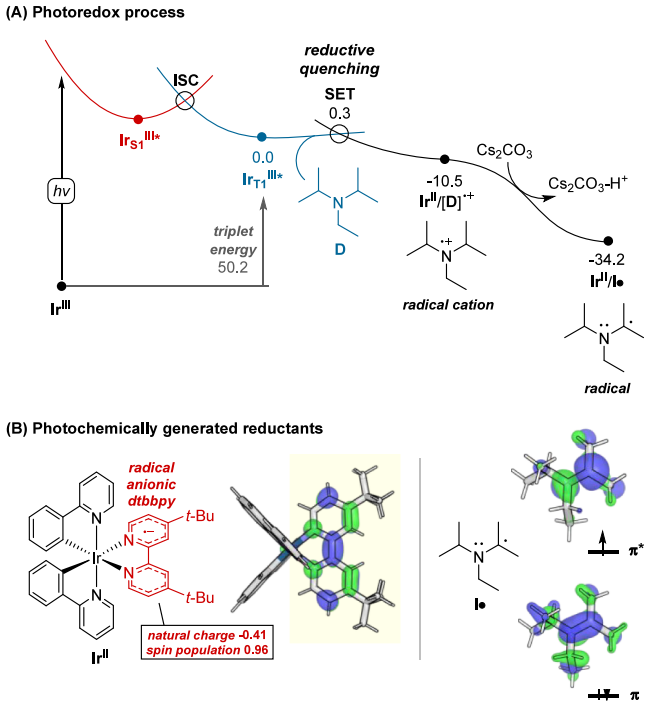

Figure 1. Computational insights into the photoredox cycle. All free energies are in kcal/mol.

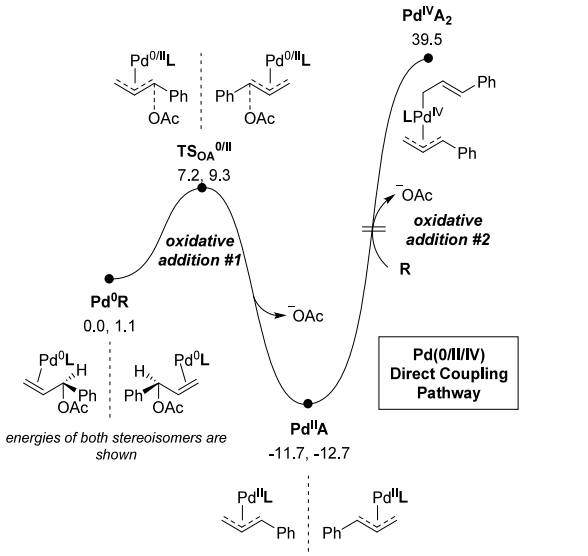

Figure 2. Free energy profile for Pd(0/II/IV) direct coupling (unit: kcal/mol, energy zero: lower-energy stereoisomer of **Pd^{0}R**).

several potentially competitive pathways, including the quenching of **Ir^{III}*** by Pd(II)-allyl species, were computed to be less favorable (Figures S2 and S3). These results support the Ir/DIPEA reductive quenching mechanism that was deduced from experiments.[51]

3.2. Photoredox/Pd Dual Catalysis. *3.2.1. Importance of Photoredox Chemistry.* We have delineated the visible-light-induced formation of reductants **Ir^{II}** and **I•**. How these in situ-formed reductants cooperate with the Pd catalyst to enable the selective C(sp^3)−C(sp^3) coupling remains unknown. To first demonstrate the thermochemically forbidden nature of the reaction, we modeled the consecutive oxidative additions (OAs) of two molecules of allylic esters with Pd(0). As described in Figure 2, this would furnish the high-valent bis(allyl)Pd(IV) species **Pd^{IV}A$_2$**. Our calculations show that the first substrate uptake can occur smoothly via an antidisplacement-type Pd(0)/Pd(II) OA, giving rise to (π-allyl)Pd(II) species **Pd^{II}A**. The reaction has a low kinetic barrier (<10 kcal/mol via **TS$_{OA}^{0/II}$**) and is exergonic (ca. −12 kcal/mol for **Pd^{II}A** vs **Pd^{0}R**). However, the Pd(II)/Pd(IV) OA, which would afford the high-valent bis(allyl)Pd(IV) species **Pd^{IV}A$_2$**, displays a prohibitively high energy of 52.2 kcal/mol (vs the more stable stereoisomer of **Pd^{II}A**). Hence, the Pd(0/II/IV) pathway is not energetically favorable, which highlights the importance of photoredox chemistry for the coupling.

3.2.2. Radical Generation. We then explored possible intersections of Pd catalysis with the photoredox system. Previous mechanistic studies suggested that both allyl radical and allylpalladium are formed during catalysis,[51] but the nature of the radical generation pathway remains unclear. With this question in mind, we proposed a Pd(0/II/I) radical generation cycle, whose energetics were calculated as presented in Figure 3A. Intriguingly, the one-electron reduction of **Pd^{II}A** by **I•** can furnish a low-valent (π-allyl)Pd(I) species **Pd^{I}A** (note: reduction by **Ir^{II}** is also feasible, see Figure S4). The detected allyl radical **A•** can then be generated from **Pd^{I}A**, possibly via the intermediacy of the **η^1-Pd^{I}A** species that is only 9.1−9.8 kcal/mol higher in energy than **Pd^{I}A**. This led us to presume an interconversion between **A•** and **Pd^{I}A** in the reaction mixture.[51]

We then explored why the low-valent allylpalladium is prone to allyl radical generation. Figure 3B presents a bonding analysis for **Pd^{II}A** and **η^3-Pd^{I}A** that reveals elongation of the internal Pd−C bond from 2.27 Å in **Pd^{II}A** to 3.01 Å in **η^3-Pd^{I}A**. Natural population analysis indicates a marked degree of ligand reduction in the allyl moiety of **η^3-Pd^{I}A**, with −0.45 partial charge and 0.66 spin population. The high-energy electron accepted by **Pd^{II}A** occupies an antibonding orbital exhibiting mixed characters of Pd $d_{x^2-y^2}$ and allyl π_2 orbitals (left in Figure 3C), which can undermine the Pd-allyl bonding interactions. The radical generation allows the extra electron to occupy a nonbonding π_2 orbital in **A•** instead (right in Figure 3C), resulting in stabilizations that we postulate to be a crucial driving force for radical generation.

Notably, the predicted generation of the highly reactive allyl radicals necessitates a mechanism that can rapidly intercept the radicals in order to avoid nonselective radical−radical coupling pathways.[59−64] How the chiral Pd catalyst overcomes this challenge and achieves strong stereodifferentiation is explored in the following sections.

3.2.3. Interception of Allyl Radicals. While the above analysis has established a consensus between theory and experiments regarding the radical generation, the relationship between the Pd(0/II/I) radical generation cycle and highly selective C(sp^3)−C(sp^3) bond construction is not yet understood. Several mechanistic questions remain to be addressed, such as whether the generation of allyl radical is only a by-pathway or else a necessary step for bond formation, whether there exist other substrate activation modes that might be utilized in the future for cross-coupling, and how the catalytic components work in synergy to achieve selective bond formation and their individual roles in this process. Answering these questions requires exploring an array of possible bond-

https://doi.org/10.1021/jacs.4c00676
J. Am. Chem. Soc. 2024, 146, 6377−6387

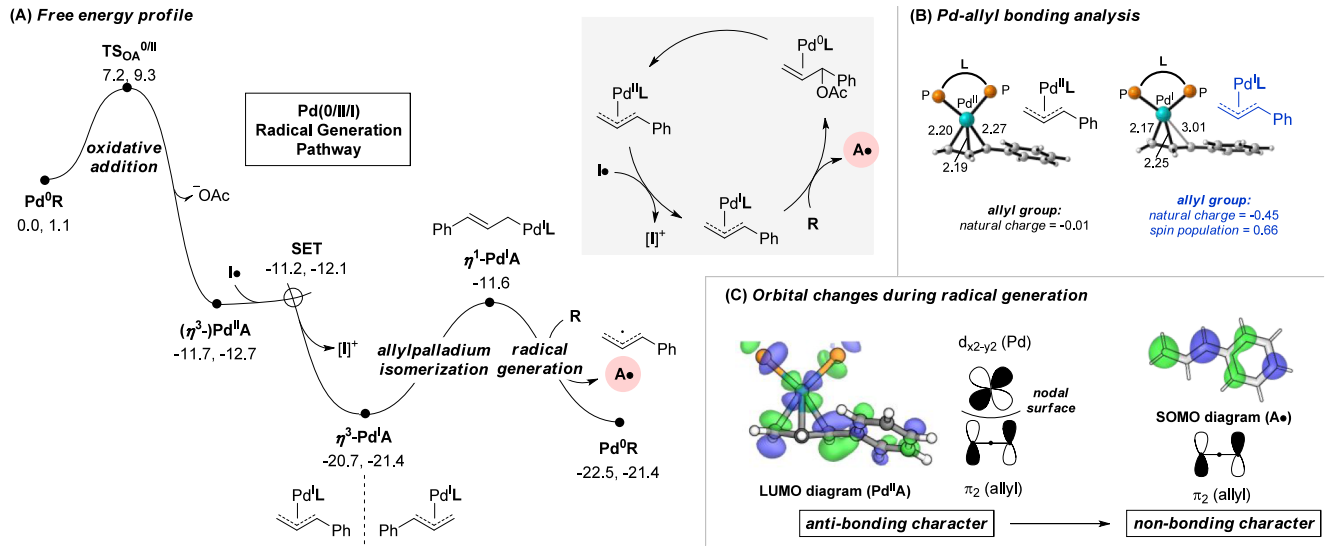

Figure 3. Mechanism of radical generation. (A) Free energy profile for the Pd(0/II/I) radical generation cycle (unit: kcal/mol, energy zero: lower-energy stereoisomer of **Pd^{0}R**). (B) Geometric and natural population analysis for Pd-allyl bonding. Bonding distances are shown in Å. (C) Changes of relevant frontier molecular orbitals during radical generation.

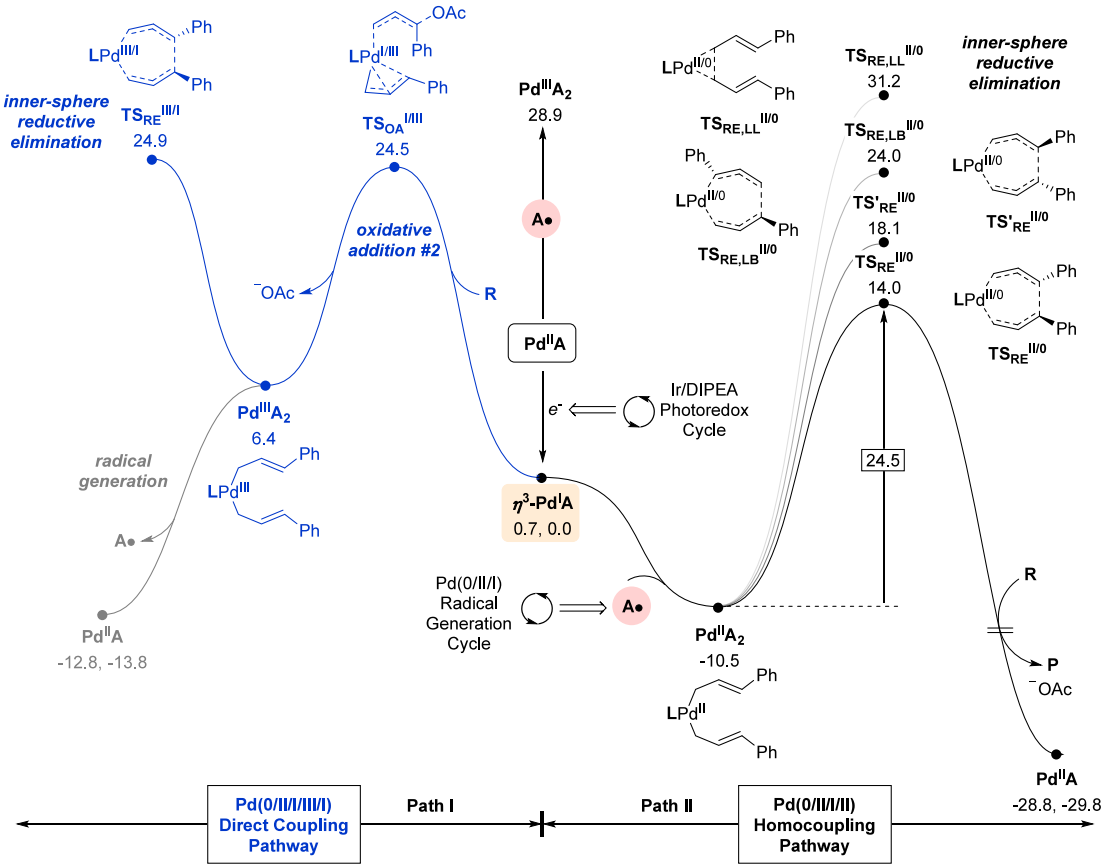

Figure 4. Free energy profiles for inner-sphere mechanisms of C(sp^3)−C(sp^3) bond formation (unit: kcal/mol). Note that the trapping of **A•** by **Pd^{II}A** forms a bis(allyl)Pd(III) species, which is 39.4 kcal/mol higher than **Pd^{II}A$_2$**, excluding the Pd(0)/Pd(II)/Pd(III)/Pd(I) and Pd(0)/Pd(II)/Pd(III)/Pd(II) pathways.

formation mechanisms that represent different modes of photoredox/Pd cooperativity.

We begin by investigating path **I**, which represents the possibility that η^3-**Pd^{I}A** primarily interacts with **R** in subsequent steps (left, Figure 4). This implies that the radical generation is only a by-pathway, and **A•** is not directly utilized for bond formation. As depicted in Figure 4, **Pd^{I}A** can undergo a Pd(I)/Pd(III) OA to afford the bis(allyl)Pd(III) species **Pd^{III}A$_2$** ($\Delta G_{OA}^{\ddagger}$ = 24.5 kcal/mol). Although the product can then be furnished from **Pd^{III}A$_2$** via Pd(III)/Pd(I) RE with a total barrier of 24.9 kcal/mol, we notice that **Pd^{III}A$_2$** is more prone to Pd−allyl homolysis, leading to the preferential

https://doi.org/10.1021/jacs.4c00676
J. Am. Chem. Soc. 2024, 146, 6377−6387

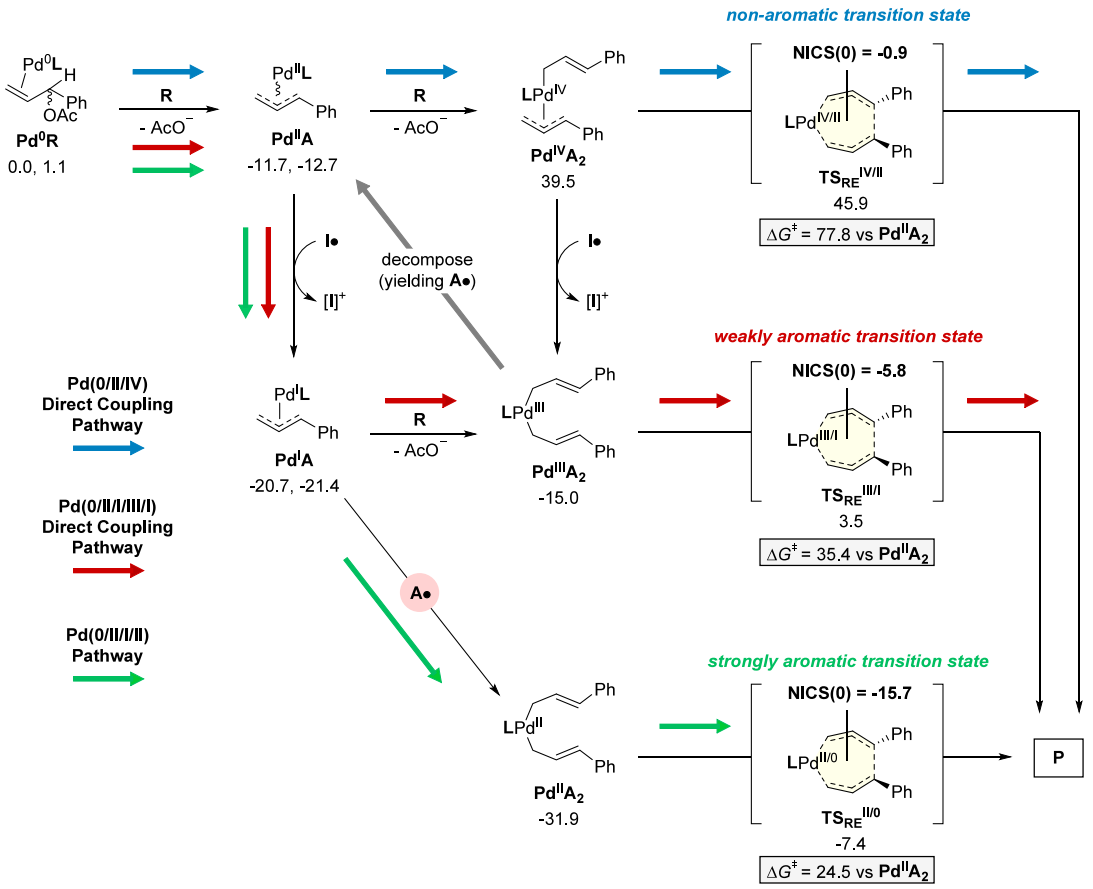

Figure 5. Synergistic photoredox/Pd reaction network. Free energies of the key species are shown in kcal/mol. NICS(0) is provided in parts per million for key bond-forming transition states.

formation of $\mathbf{Pd^{II}A}$ and **A•**, which would become a low-energy resting state. The total barrier from the resting state of dissociated $\mathbf{Pd^{II}A}$ and **A•** to $\mathbf{TS_{RE}^{III/I}}$ is nearly 40 kcal/mol, making it inaccessible.

In contrast to path **I**, an alternative hypothesis is that **A•** is a major allyl source to interact with $\boldsymbol{\eta^3}$-$\mathbf{Pd^{I}A}$ (path **II**, right in Figure 4). In fact, coordination of **A•** to allylpalladium can yield a bis(allyl)Pd intermediate, whose reductive elimination holds the potential of creating the observed regio-/stereoselectivities. Indeed, this is reflected by the lower-energy pathway in Figure 4 where $\boldsymbol{\eta^3}$-$\mathbf{Pd^{I}A}$, which contains an unpaired electron that strongly desires bonding, readily binds **A•** with a potent free energy change of ca. −11 kcal/mol. Notably, the resulting bis(allyl)Pd(II) intermediate $\mathbf{Pd^{II}A_2}$ is known to undergo facile inner-sphere RE.[89−96] This bond-forming step is computed to be rate-limiting, showing an accessible barrier of 24.5 kcal/mol, which indicates a considerable energetic advantage over path **I**. The results emphasize the preference for the low-valent Pd pathway over the high-valent alternatives.

Calculations based on the Pd(0/II/I/II) bond-forming mechanism can perfectly predict the selectivities.[51] The chiral ligand can create a high degree of asymmetric induction when adopting the Pd(II)/Pd(0) inner-sphere transition state models, leading to a considerable preference toward the major enantiomer **P** (via $\mathbf{TS_{RE}^{II/0}}$) than the opposite enantiomer **P′** (via $\mathbf{TS_{RE}^{II/0}}$, 4.1 kcal/mol higher). Formation of the branched/branched product is strongly favored over linear/branched (via $\mathbf{TS_{RE,LB}^{II/0}}$, 10.0 kcal/mol higher) and linear/linear products (via $\mathbf{TS_{RE,LL}^{II/0}}$, 17.2 kcal/mol higher), which is again consistent with experiments. Hence, the proposed inner-sphere pathway is in stark contrast to nonselective radical−radical coupling pathways,[59−64] which underscores that the rapid interception of the in situ-formed allyl radicals by Pd(I)-allyl species is a key prerequisite for the selective asymmetric bond construction.[65]

Combined, the evidence presented here implicates the tandem operations of a Pd(0/II/I) radical generation cycle and a Pd(0/II/I/II) homocoupling cycle. The latter cycle intercepts the allyl radical generated from the former, installs it onto a low-valent (π-allyl)Pd(I) species to furnish bis(allyl)-Pd(II) intermediate, and regio-/stereoselectively constructs the $C(sp^3)-C(sp^3)$ bond.

3.2.4. Reaction Network Analysis. We have examined two representative inner-sphere bond-forming pathways that are supportive of a Pd(0/II/I/II) cycle. However, other combinations of intermediate (photo)redox events with bond formation remain underexplored. To offer a more complete understanding, we present the entire photoredox/Pd reaction network for inner-sphere bond formation in Figure 5A. From left to right, the figure illustrates the progression from allylpalladium-forming oxidative addition to generation of bis(allyl)Pd species and finally to allyl−allyl bond formation. The species involved in each column are depicted in decreasing oxidation states from top to bottom. Of note, when following Pd(0/II/I/II) pathway (indicated by red

https://doi.org/10.1021/jacs.4c00676
J. Am. Chem. Soc. 2024, 146, 6377−6387

Scheme 2. Proposed Mechanism of Photoredox/Pd Dual Catalysis

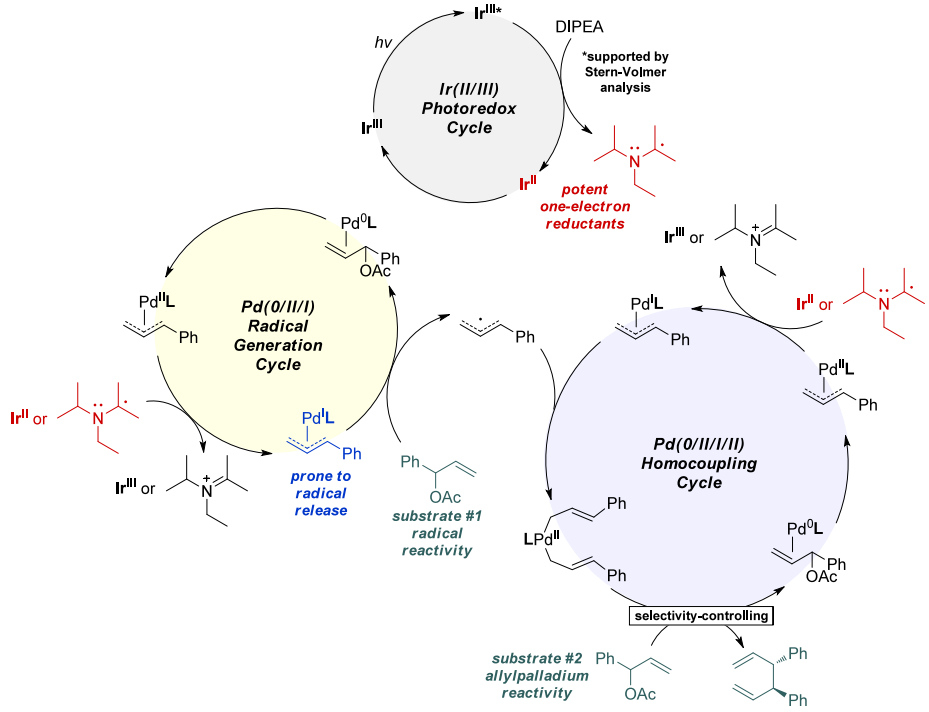

arrows), the sequential formations of $\mathbf{Pd^{II}A}$, $\mathbf{Pd^{I}A}$, and $\mathbf{Pd^{II}A_2}$ occur exergonically. Subsequently, a low-barrier inner-sphere reductive elimination takes place smoothly via $\mathbf{TS_{RE}^{II/0}}$. In contrast, all other product-forming pathways involve high-energy intermediates ($\mathbf{Pd^{IV}A_2}$ or $\mathbf{Pd^{III}A_2}$) or transition states ($\mathbf{TS_{RE}^{IV/II}}$ or $\mathbf{TS_{RE}^{III/I}}$), making them less favorable or even prohibitive. Intriguingly, our further nucleus-independent chemical shift (NICS) calculations reveal that the elevated Pd oxidation states in $\mathbf{TS_{RE}^{III/I}}$ and $\mathbf{TS_{RE}^{IV/II}}$ result in weakly and nonaromatic high-valent transition states, respectively, which contrast the strong aromaticity of the low-valent $\mathbf{TS_{RE}^{II/0}}$ (see details in Figure S5).

3.2.5. Outer-Sphere Bond Formation. To further validate the inner-sphere mechanism, we also examined the competing outer-sphere radical-attack pathways (Figure S6). Briefly, we found that the outer-sphere radical-attack TS toward the correct product is higher in energy than the inner-sphere $\mathbf{TS_{RE}^{II/0}}$ by more than 18 kcal/mol. Also, the radical-attack TSs result incorrectly predicts selectivities. These results exclude the outer-sphere bond-formation model, strengthening our proposed mechanism.

3.2.6. Completed Catalytic Cycle. Scheme 2 summarizes our main mechanistic conclusions, which involve a sophisticated interplay between the Ir/DIPEA photoredox and Pd catalysis, with the simultaneous operation of (1) an Ir/DIPEA photoredox cycle, (2) a Pd(0/II/I) radical generation cycle, and (3) a Pd(0/II/I/II) homocoupling cycle. Compared with related thermal reactions,[89−96] the access to a key bis(allyl)-Pd(II) species is realized here through a mixed mode of substrate activation, whereby a pair of allyl units are installed onto a Pd center via (1) Pd(0)/Pd(II) oxidative addition and (2) radical coordination. These mechanistically divergent activation modes constitute a salient feature of dual-catalytic photoredox/Pd homocoupling that implies an opportunity for realizing reductive cross-coupling. The resulting bis(allyl)Pd-(II) species undergoes a unique pericyclic reductive elimination via an inner-sphere, aromatic transition structure to allow selective $C(sp^3)-C(sp^3)$ bond formation, which is the rate-determining step. The results highlight the critical involvement of low-valent Pd species in rapidly trapping the in situ-generated radicals and thereby enabling the catalysis.

3.3. Origin of Selectivities. There has been extensive research on the regiochemistry of allylic substitution, particularly the switchable site selectivity for the nucleophilic displacements of allylpalladium species.[97−100] Even so, few studies have examined the factors underlying the regioselectivity of bis(allyl)Pd^{II} reductive coupling, which is highly relevant for constructing sterically congested $C(sp^3)-C(sp^3)$ bonds from allylic electrophiles. The current photoredox/Pd dual-catalytic homocoupling shows excellent regiocontrol, favoring the branched/branched 1,5-diene $\mathbf{P_{BB}}$ over the alternative linear/branched and linear/linear byproducts $\mathbf{P_{BL}}$ and $\mathbf{P_{LL}}$. Nonetheless, previous research on allylpalladium regiochemistry focused on electrophilic displacements in outer-sphere pathways. The current system also shows particularly high enantioselectivity of the current system (up to 99% *ee*) as compared to the reported stereoinduction models for similar transition states.[90−93] Understanding these selectivities might offer a molecular view for future catalyst design and optimization.

To rationalize these observations and to further validate our proposed mechanism, we utilized the standard reactions shown in Scheme 1A to calculate the competing transition states, as illustrated in Figure 6A. Here, $\mathbf{TS_{RE,LR}^{II/0}}$/$\mathbf{TS_{RE,LR}^{II/0}}$ are the linear/branched analogues of $\mathbf{TS_{RE}^{II/0}}$/$\mathbf{TS_{RE}^{II}}$, respectively, and $\mathbf{TS_{RE,LL}^{II/0}}$ leads to a linear/linear product via a conventional three-membered-ring TS. Our computations unambiguously predicted the formation of branched/branched products with the correct stereochemistry. A more detailed examination allowed

https://doi.org/10.1021/jacs.4c00676
J. Am. Chem. Soc. 2024, 146, 6377−6387

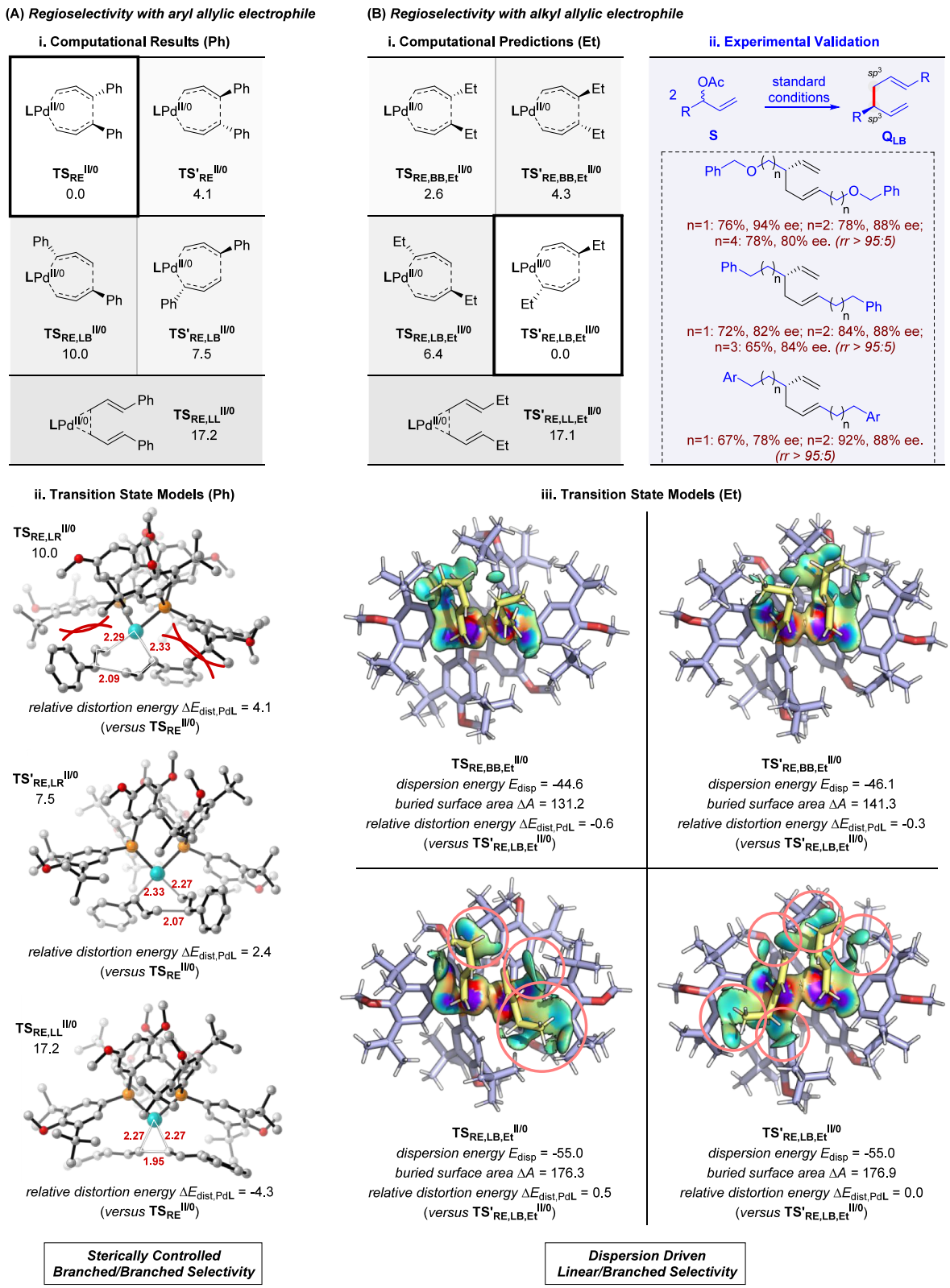

Figure 6. Origin of regioselectivity. (A) Sterically controlled branched/branched selectivity with an aryl allylic electrophile. (B) Dispersion-driven linear/branched selectivity with an alkyl allylic electrophile and experimental validations under standard conditions. All energies (relative barriers, dispersion interaction energies, and distortion energies) are shown in kcal/mol and areas in Å^2.

us to identify steric hindrance as a prominent contributor to the observed selectivity.[101,102]

To validate our computational model and investigate the impact of substrate class on regioselectivity, we predicted the reaction outcome when an alkyl allylic ester, **S**, is used instead of the aryl allylic electrophile, **R** (Figure 6B). In contrast to the excellent branched/branched selectivity observed for **R**, our computational models predict that **S** will exclusively result in

https://doi.org/10.1021/jacs.4c00676
J. Am. Chem. Soc. 2024, 146, 6377−6387

the formation of linear/branched product $\mathbf{Q_{LB}}$ with a $\Delta\Delta G^{\ddagger}$ value of at least 2.6 kcal/mol. Notably, this prediction is validated by experimental outcomes for a range of alkyl-substituted substrates under the standard conditions to give the expected products in high yields (65−93%), good enantioselectivity (78−94% *ee*), and excellent regioselectivity (>95:5 *rr*).[59] Intriguingly, we found that the flexible alkyl group adaptively avoids potential steric conflicts with the ligand, allowing for a congested linear-branched transition state. Moreover, the alkyl group allows extensive dispersion attraction within the inner pocket of the sizable chiral ligand.[101−105] Collectively, these analyses reveal a substrate-dependent interplay between dispersion and steric effects that dictate regio- and stereoselectivities in the current inner-sphere bond-formation mechanism.

4. CONCLUSION

We have utilized a combination of quantum mechanical computations and substrate-dependent experiments to investigate the mechanism of the asymmetric photoredox/Pd dual-catalytic $C(sp^3)-C(sp^3)$ homocoupling of allylic electrophiles.[51] In stark contrast to the prevailing hypothesis that high-valent Pd(III) or Pd(IV) is responsible for promoting bond formation via reductive elimination,[35,37,54−57,59−63] we have established a unique low-valent allylpalladium chemistry in photoredox/Pd dual catalysis. We further propose dual roles of the low-valent allylpalladium in the following two tandem cycles:

- a Pd(0/II/I) radical-generation cycle, which activates the allylic ester to form nonchiral allyl radicals,
- a Pd(0/II/I/II) bond-formation cycle, where the Pd catalyst activates another molecule of allylic ester, intercepts an in situ-generated allyl radical, and orchestrates the highly selective $C(sp^3)-C(sp^3)$ homocoupling through reductive elimination from a Pd(II) center.

Remarkably, for the latter cycle, we have elucidated an inner-sphere mechanism for the seven-membered-ring pericyclic reductive elimination from bis(allyl)Pd species,[89] which results in (a) the preference for low-valent Pd and (b) the exclusive regio- and stereoselectivities during the bond-forming step. This effectively avoids nonselective radical−radical coupling pathways,[59−64] underscoring the promising use of low-valent allylpalladium chemistry in intercepting transient radicals for selective $C(sp^3)-C(sp^3)$ bond constructions.[65] We have also established predictive models for regio- and stereoselectivities, which feature a substrate-dependent interplay between dispersion effects and steric repulsion.[101,102] In summary, the study is anticipated to find values in the design and rationalization of synergistic photoredox/transition-metal dual catalysis.

■ ASSOCIATED CONTENT

Supporting Information

The Supporting Information is available free of charge at https://pubs.acs.org/doi/10.1021/jacs.4c00676.

Computational and experimental results; general procedure for the synthesis of products **2** and characterization; energies and Cartesian coordinates of optimized structures; NMR spectra of synthesized compounds; photoexcitation of $\mathbf{Ir^{III}}$ species (Figure S1); Ir^{III}/Pd^{II}-allyl quenching pathways (Figure S2); $\mathbf{Ir^{III}}$*/DIPEA ligand reduction pathways (Figure S3); reduction of allylpalladium $\mathbf{Pd^{II}A}$ by **I**• and **IrII** (Figure S4); transition-state bonding interactions in reductive elimination (Figure S5); calculations for outer-sphere bond-formation pathway (Figure S6), direct Pd(0/II/IV) coupling pathway (Figure S7), radical generation pathway (Figure S8), $C(sp^3)-C(sp^3)$ coupling pathway (Figure S9); screening of the chiral ligands and the reductant (Tables S1 and S2) (PDF)

■ AUTHOR INFORMATION

Corresponding Authors

Shouyun Yu − *State Key Laboratory of Analytical Chemistry for Life Science, Jiangsu Key Laboratory of Advanced Organic Materials, Chemistry and Biomedicine Innovation Center (ChemBIC), School of Chemistry and Chemical Engineering, Nanjing University, Nanjing 210023, People's Republic of China*; orcid.org/0000-0003-4292-4714; Email: yushouyun@nju.edu.cn

William A. Goddard III − *Materials and Process Simulation Center, Beckman Institute, California Institute of Technology, Pasadena, California 91125, United States*; Email: wag@caltech.edu

Yanfeng Dang − *Tianjin Key Laboratory of Molecular Optoelectronic Sciences, Department of Chemistry, School of Science, Tianjin University, Tianjin 300072, China*; orcid.org/0000-0002-9297-9759; Email: yanfeng.dang@tju.edu.cn

Authors

Bo Li − *Tianjin Key Laboratory of Molecular Optoelectronic Sciences, Department of Chemistry, School of Science, Tianjin University, Tianjin 300072, China; Materials and Process Simulation Center, Beckman Institute, California Institute of Technology, Pasadena, California 91125, United States*

Hong-Hao Zhang − *State Key Laboratory of Analytical Chemistry for Life Science, Jiangsu Key Laboratory of Advanced Organic Materials, Chemistry and Biomedicine Innovation Center (ChemBIC), School of Chemistry and Chemical Engineering, Nanjing University, Nanjing 210023, People's Republic of China*

Yongrui Luo − *Key Laboratory of Organofluorine Chemistry, Shanghai Institute of Organic Chemistry, Chinese Academy of Sciences, Shanghai 200032, PR China*

Complete contact information is available at: https://pubs.acs.org/10.1021/jacs.4c00676

Author Contributions

#B.L. and H.-H.Z. contributed equally to this work.

Notes

The authors declare no competing financial interest.

■ ACKNOWLEDGMENTS

Financial support from the National Natural Science Foundation of China (Nos. 22073067, 21971110, and 22001120), the Natural Science Foundation of Jiangsu Province (No. BK20200297), and the Haihe Laboratory in Tianjin (No. 22HHXCJC00007) is acknowledged. The authors also acknowledge National Supercomputer Center in Tianjin, where the calculations were performed on Tianhe 3F. W.A.G. thanks the US National Science Foundation for support (CBET 2311117, Robert McCabe, prog. Mgr.).

REFERENCES

(1) Fu, G. C. Transition-Metal Catalysis of Nucleophilic Substitution Reactions: A Radical Alternative to S_N and S_N Processes. *ACS Cent. Sci.* **2017**, *3* (7), 692−700.

(2) Choi, J.; Fu, G. C. Transition Metal−Catalyzed Alkyl-Alkyl Bond Formation: Another Dimension in Cross-Coupling Chemistry. *Science* **2017**, *356* (6334), No. eaaf7230.

(3) Geist, E.; Kirschning, A.; Schmidt, T. sp3-sp3 Coupling Reactions in the Synthesis of Natural Products and Biologically Active Molecules. *Nat Prod. Rep.* **2014**, *31* (4), 441.

(4) Rudolph, A.; Lautens, M. Secondary Alkyl Halides in Transition-Metal-Catalyzed Cross-Coupling Reactions. *Angew. Chem. Int. Ed.* **2009**, *48* (15), 2656−2670.

(5) Cherney, A. H.; Kadunce, N. T.; Reisman, S. E. Enantioselective and Enantiospecific Transition-Metal-Catalyzed Cross-Coupling Reactions of Organometallic Reagents To Construct C−C Bonds. *Chem. Rev.* **2015**, *115* (17), 9587−9652.

(6) Swift, E. C.; Jarvo, E. R. Asymmetric Transition Metal-Catalyzed Cross-Coupling Reactions for the Construction of Tertiary Stereocenters. *Tetrahedron* **2013**, *69* (29), 5799−5817.

(7) Glorius, F. Asymmetric Cross-Coupling of Non-Activated Secondary Alkyl Halides. *Angew. Chem. Int. Ed.* **2008**, *47* (44), 8347−8349.

(8) Huo, H.; Gorsline, B. J.; Fu, G. C. Catalyst-Controlled Doubly Enantioconvergent Coupling of Racemic Alkyl Nucleophiles and Electrophiles. *Science* **2020**, *367* (6477), 559−564.

(9) Mu, X.; Shibata, Y.; Makida, Y.; Fu, G. C. Control of Vicinal Stereocenters through Nickel-Catalyzed Alkyl-Alkyl Cross-Coupling. *Angew. Chem. Int. Ed.* **2017**, *56* (21), 5821−5824.

(10) Schmidt, J.; Choi, J.; Liu, A. T.; Slusarczyk, M.; Fu, G. C. A General, Modular Method for the Catalytic Asymmetric Synthesis of Alkylboronate Esters. *Science* **2016**, *354* (6317), 1265−1269.

(11) Cordier, C. J.; Lundgren, R. J.; Fu, G. C. Enantioconvergent Cross-Couplings of Racemic Alkylmetal Reagents with Unactivated Secondary Alkyl Electrophiles: Catalytic Asymmetric Negishi α-Alkylations of *N* -Boc-Pyrrolidine. *J. Am. Chem. Soc.* **2013**, *135* (30), 10946−10949.

(12) Binder, J. T.; Cordier, C. J.; Fu, G. C. Catalytic Enantioselective Cross-Couplings of Secondary Alkyl Electrophiles with Secondary Alkylmetal Nucleophiles: Negishi Reactions of Racemic Benzylic Bromides with Achiral Alkylzinc Reagents. *J. Am. Chem. Soc.* **2012**, *134* (41), 17003−17006.

(13) Son, S.; Fu, G. C. Nickel-Catalyzed Asymmetric Negishi Cross-Couplings of Secondary Allylic Chlorides with Alkylzincs. *J. Am. Chem. Soc.* **2008**, *130* (9), 2756−2757.

(14) Saito, B.; Fu, G. C. Enantioselective Alkyl−Alkyl Suzuki Cross-Couplings of Unactivated Homobenzylic Halides. *J. Am. Chem. Soc.* **2008**, *130* (21), 6694−6695.

(15) Fischer, C.; Fu, G. C. Asymmetric Nickel-Catalyzed Negishi Cross-Couplings of Secondary α-Bromo Amides with Organozinc Reagents. *J. Am. Chem. Soc.* **2005**, *127* (13), 4594−4595.

(16) Poremba, K. E.; Dibrell, S. E.; Reisman, S. E. Nickel-Catalyzed Enantioselective Reductive Cross-Coupling Reactions. *ACS Catal.* **2020**, *10* (15), 8237−8246.

(17) Lucas, E. L.; Jarvo, E. R. Stereospecific and Stereoconvergent Cross-Couplings between Alkyl Electrophiles. *Nat. Rev. Chem.* **2017**, *1* (9), 0065.

(18) Wang, X.; Dai, Y.; Gong, H. Nickel-Catalyzed Reductive Couplings. *Top Curr. Chem.* **2016**, *374* (4), 43.

(19) Weix, D. J. Methods and Mechanisms for Cross-Electrophile Coupling of Csp^2 Halides with Alkyl Electrophiles. *Acc. Chem. Res.* **2015**, *48* (6), 1767−1775.

(20) Gu, J.; Wang, X.; Xue, W.; Gong, H. Nickel-Catalyzed Reductive Coupling of Alkyl Halides with Other Electrophiles: Concept and Mechanistic Considerations. *Org. Chem. Front.* **2015**, *2* (10), 1411−1421.

(21) Moragas, T.; Correa, A.; Martin, R. Metal-Catalyzed Reductive Coupling Reactions of Organic Halides with Carbonyl-Type Compounds. *Chem. Eur. J.* **2014**, *20* (27), 8242−8258.

(22) Chen, P.-P.; McGinnis, T. M.; Lin, P. C.; Hong, X.; Jarvo, E. R. A Nickel-Catalyzed Cross-Electrophile Coupling Reaction of 1,3-Dimesylates for Alkylcyclopropane Synthesis: Investigation of Stereochemical Outcomes and Radical Lifetimes. *ACS Catal.* **2023**, *13* (8), 5472−5481.

(23) Sanford, A. B.; Thane, T. A.; McGinnis, T. M.; Chen, P.-P.; Hong, X.; Jarvo, E. R. Nickel-Catalyzed Alkyl−Alkyl Cross-Electrophile Coupling Reaction of 1,3-Dimesylates for the Synthesis of Alkylcyclopropanes. *J. Am. Chem. Soc.* **2020**, *142* (11), 5017−5023.

(24) Chen, H.; Jia, X.; Yu, Y.; Qian, Q.; Gong, H. Nickel-Catalyzed Reductive Allylation of Tertiary Alkyl Halides with Allylic Carbonates. *Angew. Chem. Int. Ed.* **2017**, *56* (42), 13103−13106.

(25) Erickson, L. W.; Lucas, E. L.; Tollefson, E. J.; Jarvo, E. R. Nickel-Catalyzed Cross-Electrophile Coupling of Alkyl Fluorides: Stereospecific Synthesis of Vinylcyclopropanes. *J. Am. Chem. Soc.* **2016**, *138* (42), 14006−14011.

(26) Wang, X.; Wang, S.; Xue, W.; Gong, H. Nickel-Catalyzed Reductive Coupling of Aryl Bromides with Tertiary Alkyl Halides. *J. Am. Chem. Soc.* **2015**, *137* (36), 11562−11565.

(27) Tollefson, E. J.; Erickson, L. W.; Jarvo, E. R. Stereospecific Intramolecular Reductive Cross-Electrophile Coupling Reactions for Cyclopropane Synthesis. *J. Am. Chem. Soc.* **2015**, *137* (31), 9760−9763.

(28) Kadunce, N. T.; Reisman, S. E. Nickel-Catalyzed Asymmetric Reductive Cross-Coupling between Heteroaryl Iodides and α-Chloronitriles. *J. Am. Chem. Soc.* **2015**, *137* (33), 10480−10483.

(29) Cherney, A. H.; Reisman, S. E. Nickel-Catalyzed Asymmetric Reductive Cross-Coupling Between Vinyl and Benzyl Electrophiles. *J. Am. Chem. Soc.* **2014**, *136* (41), 14365−14368.

(30) Cherney, A. H.; Kadunce, N. T.; Reisman, S. E. Catalytic Asymmetric Reductive Acyl Cross-Coupling: Synthesis of Enantioenriched Acyclic α,α-Disubstituted Ketones. *J. Am. Chem. Soc.* **2013**, *135* (20), 7442−7445.

(31) Wang, S.; Qian, Q.; Gong, H. Nickel-Catalyzed Reductive Coupling of Aryl Halides with Secondary Alkyl Bromides and Allylic Acetate. *Org. Lett.* **2012**, *14* (13), 3352−3355.

(32) Yu, X.; Yang, T.; Wang, S.; Xu, H.; Gong, H. Nickel-Catalyzed Reductive Cross-Coupling of Unactivated Alkyl Halides. *Org. Lett.* **2011**, *13* (8), 2138−2141.

(33) Prinsell, M. R.; Everson, D. A.; Weix, D. J. Nickel-Catalyzed Sodium Iodide-Promoted Reductive Dimerization of Alkyl Halides, Alkyl Pseudohalides, and Allylic Acetates. *Chem. Commun.* **2010**, *46* (31), 5743.

(34) Zhu, C.; Yue, H.; Chu, L.; Rueping, M. Recent Advances in Photoredox and Nickel Dual-Catalyzed Cascade Reactions: Pushing the Boundaries of Complexity. *Chem. Sci.* **2020**, *11* (16), 4051−4064.

(35) De Abreu, M.; Belmont, P.; Brachet, E. Synergistic Photoredox/Transition-Metal Catalysis for Carbon−Carbon Bond Formation Reactions. *Eur. J. Org. Chem.* **2020**, *2020* (10), 1327−1378.

(36) Milligan, J. A.; Phelan, J. P.; Badir, S. O.; Molander, G. A. Alkyl Carbon−Carbon Bond Formation by Nickel/Photoredox Cross-Coupling. *Angew. Chem. Int. Ed.* **2019**, *58* (19), 6152−6163.

(37) Twilton, J.; Le, C.; Zhang, P.; Shaw, M. H.; Evans, R. W.; MacMillan, D. W. C. The Merger of Transition Metal and Photocatalysis. *Nat. Rev. Chem.* **2017**, *1* (7), 0052.

(38) Tellis, J. C.; Kelly, C. B.; Primer, D. N.; Jouffroy, M.; Patel, N. R.; Molander, G. A. Single-Electron Transmetalation via Photoredox/Nickel Dual Catalysis: Unlocking a New Paradigm for Sp^3−Sp^2 Cross-Coupling. *Acc. Chem. Res.* **2016**, *49* (7), 1429−1439.

(39) Skubi, K. L.; Blum, T. R.; Yoon, T. P. Dual Catalysis Strategies in Photochemical Synthesis. *Chem. Rev.* **2016**, *116* (17), 10035−10074.

(40) Zheng, P.; Zhou, P.; Wang, D.; Xu, W.; Wang, H.; Xu, T. Dual Ni/Photoredox-Catalyzed Asymmetric Cross-Coupling to Access Chiral Benzylic Boronic Esters. *Nat. Commun.* **2021**, *12* (1), 1646.

(41) Steiman, T. J.; Liu, J.; Mengiste, A.; Doyle, A. G. Synthesis of β-Phenethylamines via Ni/Photoredox Cross-Electrophile Coupling of Aliphatic Aziridines and Aryl Iodides. *J. Am. Chem. Soc.* **2020**, *142* (16), 7598−7605.

https://doi.org/10.1021/jacs.4c00676
J. Am. Chem. Soc. 2024, 146, 6377−6387

(42) Song, F.; Wang, F.; Guo, L.; Feng, X.; Zhang, Y.; Chu, L. Visible-Light-Enabled Stereodivergent Synthesis of *E* - and *Z* -Configured 1,4-Dienes by Photoredox/Nickel Dual Catalysis. *Angew. Chem.* **2020**, *132* (1), 183−187.
(43) Parasram, M.; Shields, B. J.; Ahmad, O.; Knauber, T.; Doyle, A. G. Regioselective Cross-Electrophile Coupling of Epoxides and (Hetero)Aryl Iodides via Ni/Ti/Photoredox Catalysis. *ACS Catal.* **2020**, *10* (10), 5821−5827.
(44) Guan, H.; Zhang, Q.; Walsh, P. J.; Mao, J. Nickel/Photoredox-Catalyzed Asymmetric Reductive Cross-Coupling of Racemic α-Chloro Esters with Aryl Iodides. *Angew. Chem. Int. Ed.* **2020**, *59* (13), 5172−5177.
(45) Dewanji, A.; Bülow, R. F.; Rueping, M. Photoredox/Nickel Dual-Catalyzed Reductive Cross Coupling of Aryl Halides Using an Organic Reducing Agent. *Org. Lett.* **2020**, *22* (4), 1611−1617.
(46) Yu, W.; Chen, L.; Tao, J.; Wang, T.; Fu, J. Dual Nickel- and Photoredox-Catalyzed Reductive Cross-Coupling of Aryl Vinyl Halides and Unactivated Tertiary Alkyl Bromides. *Chem. Commun.* **2019**, *55* (42), 5918−5921.
(47) Yi, J.; Badir, S. O.; Kammer, L. M.; Ribagorda, M.; Molander, G. A. Deaminative Reductive Arylation Enabled by Nickel/Photoredox Dual Catalysis. *Org. Lett.* **2019**, *21* (9), 3346−3351.
(48) Smith, R. T.; Zhang, X.; Rincón, J. A.; Agejas, J.; Mateos, C.; Barberis, M.; García-Cerrada, S.; De Frutos, O.; MacMillan, D. W. C. Metallaphotoredox-Catalyzed Cross-Electrophile C_{sp^3}−C_{sp^3} Coupling of Aliphatic Bromides. *J. Am. Chem. Soc.* **2018**, *140* (50), 17433−17438.
(49) Peng, L.; Li, Z.; Yin, G. Photochemical Nickel-Catalyzed Reductive Migratory Cross-Coupling of Alkyl Bromides with Aryl Bromides. *Org. Lett.* **2018**, *20* (7), 1880−1883.
(50) Zhang, P.; Le, C.; MacMillan, D. W. C. Silyl Radical Activation of Alkyl Halides in Metallaphotoredox Catalysis: A Unique Pathway for Cross-Electrophile Coupling. *J. Am. Chem. Soc.* **2016**, *138* (26), 8084−8087.
(51) Zhang, H.-H.; Tang, M.; Zhao, J.-J.; Song, C.; Yu, S. Enantioselective Reductive Homocoupling of Allylic Acetates Enabled by Dual Photoredox/Palladium Catalysis: Access to C_2-Symmetrical 1,5-Dienes. *J. Am. Chem. Soc.* **2021**, *143* (32), 12836−12846.
(52) Chuentragool, P.; Kurandina, D.; Gevorgyan, V. Catalysis with Palladium Complexes Photoexcited by Visible Light. *Angew. Chem. Int. Ed.* **2019**, *58* (34), 11586−11598.
(53) Zhang, H.-H.; Chen, H.; Zhu, C.; Yu, S. A Review of Enantioselective Dual Transition Metal/Photoredox Catalysis. *Sci. China Chem.* **2020**, *63* (5), 637−647.
(54) Chan, A. Y.; Perry, I. B.; Bissonnette, N. B.; Buksh, B. F.; Edwards, G. A.; Frye, L. I.; Garry, O. L.; Lavagnino, M. N.; Li, B. X.; Liang, Y.; Mao, E.; Millet, A.; Oakley, J. V.; Reed, N. L.; Sakai, H. A.; Seath, C. P.; MacMillan, D. W. C. Metallaphotoredox: The Merger of Photoredox and Transition Metal Catalysis. *Chem. Rev.* **2022**, *122* (2), 1485−1542.
(55) Holmberg-Douglas, N.; Nicewicz, D. A. Photoredox-Catalyzed C−H Functionalization Reactions. *Chem. Rev.* **2022**, *122* (2), 1925−2016.
(56) Mastandrea, M. M.; Pericàs, M. A. Photoredox Dual Catalysis: A Fertile Playground for the Discovery of New Reactivities. *Eur. J. Inorg. Chem.* **2021**, *2021* (34), 3421−3431.
(57) Wang, C.-S.; Dixneuf, P. H.; Soulé, J.-F. Photoredox Catalysis for Building C−C Bonds from $C(Sp^2)$−H Bonds. *Chem. Rev.* **2018**, *118* (16), 7532−7585.
(58) Huang, H.-M.; Bellotti, P.; Glorius, F. Transition Metal-Catalysed Allylic Functionalization Reactions Involving Radicals. *Chem. Soc. Rev.* **2020**, *49* (17), 6186−6197.
(59) Shee, M.; Singh, N. D. P. Cooperative Photoredox and Palladium Catalysis: Recent Advances in Various Functionalization Reactions. *Catal. Sci. Technol.* **2021**, *11* (3), 742−767.
(60) Lang, S. B.; O'Nele, K. M.; Douglas, J. T.; Tunge, J. A. Dual Catalytic Decarboxylative Allylations of α-Amino Acids and Their Divergent Mechanisms. *Chem. Eur. J.* **2015**, *21* (51), 18589−18593.
(61) Zhang, H.-H.; Zhao, J.-J.; Yu, S. Enantioselective Allylic Alkylation with 4-Alkyl-1,4-Dihydro-Pyridines Enabled by Photoredox/Palladium Cocatalysis. *J. Am. Chem. Soc.* **2018**, *140* (49), 16914−16919.
(62) Zhang, H.-H.; Zhao, J.-J.; Yu, S. Enantioselective α-Allylation of Anilines Enabled by a Combined Palladium and Photoredox Catalytic System. *ACS Catal.* **2020**, *10* (8), 4710−4716.
(63) Cartwright, K. C.; Tunge, J. A. Organophotoredox/Palladium Dual Catalytic Decarboxylative $Csp^3 - Csp^3$ Coupling of Carboxylic Acids and π-Electrophiles. *Chem. Sci.* **2020**, *11* (31), 8167−8175.
(64) Xuan, J.; Zeng, T.; Feng, Z.; Deng, Q.; Chen, J.; Lu, L.; Xiao, W.; Alper, H. Redox-Neutral α-Allylation of Amines by Combining Palladium Catalysis and Visible-Light Photoredox Catalysis. *Angew. Chem.* **2015**, *127* (5), 1645−1648.
(65) Yamano, M. M.; Kelleghan, A. V.; Shao, Q.; Giroud, M.; Simmons, B. J.; Li, B.; Chen, S.; Houk, K. N.; Garg, N. K. Intercepting Fleeting Cyclic Allenes with Asymmetric Nickel Catalysis. *Nature* **2020**, *586* (7828), 242−247.
(66) Frisch, M. J.; Trucks, G. W.; Schlegel, H. B.; Scuseria, G. E.; Robb, M. A.; Cheeseman, J. R.; Scalmani, G.; Barone, V.; Mennucci, B.; Petersson, G. A.; Nakatsuji, H.; Caricato, M.; Li, X.; Hratchian, H. P.; Izmaylov, A. F.; Bloino, J.; Zheng, G.; Sonnenberg, J. L.; Hada, M.; Ehara, M.; Toyota, K.; Fukuda, R.; Hasegawa, J.; Ishida, M.; Nakajima, T.; Honda, Y.; Kitao, O.; Nakai, H.; Vreven, T.; Montgomery, J. A., Jr; Peralta, J. E.; Ogliaro, F.; Bearpark, M.; Heyd, J. J.; Brothers, E.; Kudin, K. N.; Staroverov, V. N.; Kobayashi, R.; Normand, J.; Raghavachari, K.; Rendell, A.; Burant, J. C.; Iyengar, S. S.; Tomasi, J.; Cossi, M.; Rega, N.; Millam, N. J.; Klene, M.; Knox, J. E.; Cross, J. B.; Bakken, V.; Adamo, C.; Jaramillo, J.; Gomperts, R.; Stratmann, R. E.; Yazyev, O.; Austin, A. J.; Cammi, R.; Pomelli, C.; Ochterski, J. W.; Martin, R. L.; Morokuma, K.; Zakrzewski, V. G.; Voth, G. A.; Salvador, P.; Dannenberg, J. J.; Dapprich, S.; Daniels, A. D.; Farkas, Ö.; Foresman, J. B.; Ortiz, J. V.; Cioslowski, J.; Fox, D. J. *Gaussian 09*; Gaussian, Inc.: Wallingford, CT, 2009.
(67) Zhao, Y.; Truhlar, D. G. Density Functionals with Broad Applicability in Chemistry. *Acc. Chem. Res.* **2008**, *41* (2), 157−167.
(68) Zhao, Y.; Truhlar, D. G. The M06 Suite of Density Functionals for Main Group Thermochemistry, Thermochemical Kinetics, Noncovalent Interactions, Excited States, and Transition Elements: Two New Functionals and Systematic Testing of Four M06-Class Functionals and 12 Other Functionals. *Theor. Chem. Acc.* **2008**, *120* (1−3), 215−241.
(69) Andrae, D.; Häußermann, U.; Dolg, M.; Stoll, H.; Preuß, H. Energy-Adjustedab Initio Pseudopotentials for the Second and Third Row Transition Elements. *Theoret. Chim. Acta* **1990**, *77* (2), 123−141.
(70) Roy, L. E.; Hay, P. J.; Martin, R. L. Revised Basis Sets for the LANL Effective Core Potentials. *J. Chem. Theory Comput.* **2008**, *4* (7), 1029−1031.
(71) Weigend, F.; Ahlrichs, R. Balanced Basis Sets of Split Valence, Triple Zeta Valence and Quadruple Zeta Valence Quality for H to Rn: Design and Assessment of Accuracy. *Phys. Chem. Chem. Phys.* **2005**, *7* (18), 3297.
(72) Marenich, A. V.; Cramer, C. J.; Truhlar, D. G. Universal Solvation Model Based on Solute Electron Density and on a Continuum Model of the Solvent Defined by the Bulk Dielectric Constant and Atomic Surface Tensions. *J. Phys. Chem B* **2009**, *113* (18), 6378−6396.
(73) Luchini, G.; Alegre-Requena, J. V.; Funes-Ardoiz, I.; Paton, R. S. GoodVibes: Automated Thermochemistry for Heterogeneous Computational Chemistry Data. *F1000Research* **2020**, *9*, 291.
(74) Grimme, S. Supramolecular Binding Thermodynamics by Dispersion-Corrected Density Functional Theory. *Chem. Eur. J.* **2012**, *18* (32), 9955−9964.
(75) Li, Y.-P.; Gomes, J.; Mallikarjun Sharada, S.; Bell, A. T.; Head-Gordon, M. Improved Force-Field Parameters for QM/MM Simulations of the Energies of Adsorption for Molecules in Zeolites and a Free Rotor Correction to the Rigid Rotor Harmonic Oscillator

https://doi.org/10.1021/jacs.4c00676
J. Am. Chem. Soc. 2024, 146, 6377−6387

Model for Adsorption Enthalpies. *J. Phys. Chem. C* **2015**, *119* (4), 1840−1850.
(76) Lu, T.; Chen, F. Multiwfn: A Multifunctional Wavefunction Analyzer. *J. Comput. Chem.* **2012**, *33* (5), 580−592.
(77) Martin, R. L. Natural Transition Orbitals. *J. Chem. Phys.* **2003**, *118* (11), 4775−4777.
(78) Mayer, I. Charge Bond Order and Valence in the AB Initio SCF Theory. *Chem. Phys. Lett.* **1983**, *97* (3), 270−274.
(79) Lu, T.; Chen, F. Quantitative Analysis of Molecular Surface Based on Improved Marching Tetrahedra Algorithm. *J. Mol. Graphics Modell* **2012**, *38*, 314−323.
(80) Liu, P.; Montgomery, J.; Houk, K. N. Ligand Steric Contours To Understand the Effects of *N* -Heterocyclic Carbene Ligands on the Reversal of Regioselectivity in Ni-Catalyzed Reductive Couplings of Alkynes and Aldehydes. *J. Am. Chem. Soc.* **2011**, *133* (18), 6956−6959.
(81) Lefebvre, C.; Rubez, G.; Khartabil, H.; Boisson, J.-C.; Contreras-García, J.; Hénon, E. Accurately Extracting the Signature of Intermolecular Interactions Present in the NCI Plot of the Reduced Density Gradient versus Electron Density. *Phys. Chem. Chem. Phys.* **2017**, *19* (27), 17928−17936.
(82) Grimme, S.; Ehrlich, S.; Goerigk, L. Effect of the Damping Function in Dispersion Corrected Density Functional Theory. *J. Comput. Chem.* **2011**, *32* (7), 1456−1465.
(83) Legault, C. Y. *CYLview, 1.0b*; Université de Sherbrooke: Quebec, Montreal, Canada, 2009.
(84) Delano, W. *The PyMOL Molecular Graphics System, Version 2.6.0a0*; Schrodinger, LLC., 2010.
(85) Beatty, J. W.; Stephenson, C. R. J. Amine Functionalization via Oxidative Photoredox Catalysis: Methodology Development and Complex Molecule Synthesis. *Acc. Chem. Res.* **2015**, *48* (5), 1474−1484.
(86) Hu, J.; Wang, J.; Nguyen, T. H.; Zheng, N. The Chemistry of Amine Radical Cations Produced by Visible Light Photoredox Catalysis. *Beilstein. J. Org. Chem.* **2013**, *9*, 1977−2001.
(87) Pischel, U.; Zhang, X.; Hellrung, B.; Haselbach, E.; Muller, P.-A.; Nau, W. M. Fluorescence Quenching of n,π^*-Excited Azoalkanes by Amines: What Is a Sterically Hindered Amine? *J. Am. Chem. Soc.* **2000**, *122* (9), 2027−2034.
(88) Slinker, J. D.; Gorodetsky, A. A.; Lowry, M. S.; Wang, J.; Parker, S.; Rohl, R.; Bernhard, S.; Malliaras, G. G. Efficient Yellow Electroluminescence from a Single Layer of a Cyclometalated Iridium Complex. *J. Am. Chem. Soc.* **2004**, *126* (9), 2763−2767.
(89) Cusumano, A. Q.; Goddard, W. A.; Stoltz, B. M. The Transition Metal Catalyzed [π2s + π2s + σ2s + σ2s] Pericyclic Reaction: Woodward−Hoffmann Rules, Aromaticity, and Electron Flow. *J. Am. Chem. Soc.* **2020**, *142* (45), 19033−19039.
(90) Cusumano, A. Q.; Stoltz, B. M.; Goddard, W. A. Reaction Mechanism, Origins of Enantioselectivity, and Reactivity Trends in Asymmetric Allylic Alkylation: A Comprehensive Quantum Mechanics Investigation of a C(Sp^3)−C(Sp^3) Cross-Coupling. *J. Am. Chem. Soc.* **2020**, *142* (32), 13917−13933.
(91) McPherson, K. E.; Croatt, M. P.; Morehead, A. T.; Sargent, A. L. DFT Mechanistic Investigation of an Enantioselective Tsuji−Trost Allylation Reaction. *Organometallics* **2018**, *37* (21), 3791−3802.
(92) Ardolino, M. J.; Morken, J. P. Congested C−C Bonds by Pd-Catalyzed Enantioselective Allyl−Allyl Cross-Coupling, a Mechanism-Guided Solution. *J. Am. Chem. Soc.* **2014**, *136* (19), 7092−7100.
(93) Keith, J. A.; Behenna, D. C.; Sherden, N.; Mohr, J. T.; Ma, S.; Marinescu, S. C.; Nielsen, R. J.; Oxgaard, J.; Stoltz, B. M.; Goddard, W. A. The Reaction Mechanism of the Enantioselective Tsuji Allylation: Inner-Sphere and Outer-Sphere Pathways, Internal Rearrangements, and Asymmetric C−C Bond Formation. *J. Am. Chem. Soc.* **2012**, *134* (46), 19050−19060.
(94) Zhang, P.; Brozek, L. A.; Morken, J. P. Pd-Catalyzed Enantioselective Allyl−Allyl Cross-Coupling. *J. Am. Chem. Soc.* **2010**, *132* (31), 10686−10688.
(95) Pérez-Rodríguez, M.; Braga, A. A. C.; De Lera, A. R.; Maseras, F.; Álvarez, R.; Espinet, P. A DFT Study of the Effect of the Ligands in the Reductive Elimination from Palladium Bis(Allyl) Complexes. *Organometallics* **2010**, *29* (21), 4983−4991.
(96) Méndez, M.; Cuerva, J. M.; Gómez-Bengoa, E.; Cárdenas, D. J.; Echavarren, A. M. Intramolecular Coupling of Allyl Carboxylates with Allyl Stannanes and Allyl Silanes: A New Type of Reductive Elimination Reaction? *Chem. Eur. J.* **2002**, *8* (16), 3620.
(97) Fernandes, R. A.; Nallasivam, J. L. Catalytic Allylic Functionalization *via* π-Allyl Palladium Chemistry. *Org. Biomol. Chem.* **2019**, *17* (38), 8647−8672.
(98) Trost, B. M. Pd Asymmetric Allylic Alkylation (AAA). A Powerful Synthetic Tool. *Chem. Pharm. Bull.* **2002**, *50* (1), 1−14.
(99) Trost, B. M.; Van Vranken, D. L. Asymmetric Transition Metal-Catalyzed Allylic Alkylations. *Chem. Rev.* **1996**, *96* (1), 395−422.
(100) Trost, B. M.; Hung, M. H. On the Regiochemistry of Metal-Catalyzed Allylic Alkylation: A Model. *J. Am. Chem. Soc.* **1984**, *106* (22), 6837−6839.
(101) Li, B.; Xu, H.; Dang, Y.; Houk, K. N. Dispersion and Steric Effects on Enantio-/Diastereoselectivities in Synergistic Dual Transition-Metal Catalysis. *J. Am. Chem. Soc.* **2022**, *144* (4), 1971−1985.
(102) Li, B.; Xu, H.; Dang, Y. Dispersion Interactions in Asymmetric Induction for Constructing Vicinal Stereogenic Centers. *Acc. Chem. Res.* **2023**, *56* (22), 3260−3270.
(103) Bursch, M.; Caldeweyher, E.; Hansen, A.; Neugebauer, H.; Ehlert, S.; Grimme, S. Understanding and Quantifying London Dispersion Effects in Organometallic Complexes. *Acc. Chem. Res.* **2019**, *52* (1), 258−266.
(104) Liptrot, D. J.; Power, P. P. London Dispersion Forces in Sterically Crowded Inorganic and Organometallic Molecules. *Nat. Rev. Chem.* **2017**, *1* (1), 0004.
(105) Fanourakis, A.; Docherty, P. J.; Chuentragool, P.; Phipps, R. J. Recent Developments in Enantioselective Transition Metal Catalysis Featuring Attractive Noncovalent Interactions between Ligand and Substrate. *ACS Catal.* **2020**, *10* (18), 10672−10714.

https://doi.org/10.1021/jacs.4c00676
J. Am. Chem. Soc. 2024, 146, 6377−6387